Eur. Phys. J. C 17, 513–520 (2000)
Digital Object Identifier (DOI) 10.1007/s100520000458

THE EUROPEAN PHYSICAL JOURNAL C

The effects of Majorana phases in three-generation neutrinos

N. Haba[1,2,a], Y. Matsui[2,b], N. Okamura[3,c]

[1] Faculty of Engineering, Mie University, Tsu Mie 514-8507, Japan
[2] Department of Physics, Nagoya University, Nagoya, 464-8602, Japan
[3] Theory Group, KEK, Tsukuba Ibaraki 305-0801, Japan

Received: 9 May 2000 / Revised version: 23 May 2000 /
Published online: 8 September 2000 – © Springer-Verlag 2000

Abstract. Neutrino-oscillation solutions for the atmospheric neutrino anomaly and the solar neutrino deficit can determine the texture of the neutrino mass matrix according to three types of neutrino mass hierarchy: Type A: $m_1 \ll m_2 \ll m_3$, Type B: $m_1 \sim m_2 \gg m_3$, and Type C: $m_1 \sim m_2 \sim m_3$, where m_i is the absolute mass of the ith generation neutrino. The relative sign assignments of the neutrino masses in each type of mass hierarchy play crucial roles in the stability against quantum corrections. Actually, two physical Majorana phases in the lepton flavor mixing matrix connect the relative sign assignments of the neutrino masses. Therefore, in this paper we analyze the stability of the mixing angles against quantum corrections according to three types of neutrino mass hierarchy (Type A, B, C) and two Majorana phases. The two phases play crucial roles in the stability of the mixing angles against quantum corrections.

1 Introduction

Recent neutrino-oscillation experiments suggest strong evidence of tiny neutrino masses and lepton flavor mixings [1–3]. Studies of the lepton flavor mixing matrix, the so-called Maki–Nakagawa–Sakata (MNS) matrix [4], will give us important clues of the physics beyond the standard model. One of the most important studies is the analysis of the quantum correction of the MNS matrix [5–12].

In order to explain both the solar and the atmospheric neutrino problems, two mass-squared differences are needed,

$$\Delta m^2_{\rm solar} \equiv \left|m_2^2 - m_1^2\right| \text{ and } \quad \Delta m^2_{\rm ATM} \equiv \left|m_3^2 - m_2^2\right|, \quad (1)$$

where m_i is the ith ($i = 1$–3) generation neutrino mass ($m_i \geq 0$). $\Delta m^2_{\rm solar}$ and $\Delta m^2_{\rm ATM}$ stand for the mass squared differences of the solar neutrino [1] and the atmospheric neutrino solutions [2,3], respectively. Then there are the following three possible types of neutrino mass hierarchy [13], which are consistent with the experimental data of $\Delta m^2_{\rm solar} \ll \Delta m^2_{\rm ATM}$:

$$\begin{aligned} &\text{Type A}: \ m_1 \ll m_2 \ll m_3, \\ &\text{Type B}: \ m_1 \sim m_2 \gg m_3, \\ &\text{Type C}: \ m_1 \sim m_2 \sim m_3, \end{aligned} \quad (2)$$

where m_i is the absolute mass of the ith generation neutrino. In [10], the question has been studied whether the lepton flavor mixing angles are stable or not against quantum corrections for all three types of mass hierarchy with all considerable relative sign assignments, which are shown below, in the minimal supersymmetric standard model (MSSM) with an effective dimension-five operator which gives the Majorana masses of the neutrinos.

(i) Type A:

$$\text{case(a1)}: \quad m_\nu^{\rm a1} = \text{diag.}(0, m_2, m_3), \quad (3)$$
$$\text{case(a2)}: \quad m_\nu^{\rm a2} = \text{diag.}(0, -m_2, m_3). \quad (4)$$

$$\begin{pmatrix} m_1 = 0, \\ m_2 = \sqrt{\Delta m^2_{\rm solar}}, \\ m_3 = \sqrt{\Delta m^2_{\rm solar} + \Delta m^2_{\rm ATM}}. \end{pmatrix}$$

(ii) Type B:

$$\text{case(b1)}: \quad m_\nu^{\rm b1} = \text{diag.}(m_1, m_2, 0), \quad (5)$$
$$\text{case(b2)}: \quad m_\nu^{\rm b2} = \text{diag.}(m_1, -m_2, 0). \quad (6)$$

$$\begin{pmatrix} m_1 = \sqrt{\Delta m^2_{\rm ATM}}, \\ m_2 = \sqrt{\Delta m^2_{\rm solar} + \Delta m^2_{\rm ATM}}, \\ m_3 = 0. \end{pmatrix}$$

(iii) Type C:

$$\text{case (c1)}: \quad m_\nu^{c1} = \text{diag.}(-m_1, m_2, m_3), \quad (7)$$
$$\text{case (c2)}: \quad m_\nu^{c2} = \text{diag.}(m_1, -m_2, m_3), \quad (8)$$
$$\text{case (c3)}: \quad m_\nu^{c3} = \text{diag.}(-m_1, -m_2, m_3), \quad (9)$$
$$\text{case (c4)}: \quad m_\nu^{c4} = \text{diag.}(m_1, m_2, m_3). \quad (10)$$

[a] e-mail: haba@eken.phys.nagoya-u.ac.jp
[b] e-mail: matsui@eken.phys.nagoya-u.ac.jp
[c] e-mail: naotoshi.okamura@kek.jp

$$\begin{pmatrix} m_1 = m_0, \\ m_2 = \sqrt{m_0^2 + \Delta m^2_{\rm solar}}, \\ m_3 = \sqrt{m_0^2 + \Delta m^2_{\rm solar} + \Delta m^2_{\rm ATM}}. \end{pmatrix}$$

In [10], it has been found that the above relative sign assignments of the neutrino masses in each type play crucial roles in the stability of the mixing angles against quantum corrections. Actually, two physical Majorana phases in the lepton flavor mixing matrix connect the above relative sign assignments of the neutrino masses. Therefore, in this paper we analyze the stability of mixing angles against quantum corrections according to three types of neutrino mass hierarchy (Type A, B, C) and two Majorana phases. Two phases play crucial roles in the stability of the mixing angles against quantum corrections. In [11, 12], it has already been analyzed that the effect of a Majorana phase plays an important role in the stability against quantum corrections in two-generation neutrinos.

2 Quantum corrections to neutrino mass matrix

In the MSSM with the effective dimension-five operator which gives the Majorana masses of neutrinos, the superpotential of the lepton–Higgs interactions is given by

$$\mathcal{W} = y^{\rm e}_{ij}(H_d L_i)E_j - \frac{1}{2}\kappa_{ij}(H_u L_i)(H_u L_j). \qquad (11)$$

Here the indices i, j (= 1–3) stand for the generation number. L_i and E_i are chiral superfields of the ith generation lepton doublet and the right-handed charged lepton, respectively. H_u (H_d) is the Higgs doublet which gives Dirac masses to the up- (down-) type fermions. The neutrino mass matrix of the three generations, κ, is diagonalized by

$$U^{\rm T}\kappa\, U = D_\kappa, \qquad (12)$$

where D_κ is given by

$$D_\kappa = \begin{pmatrix} m_1 & 0 & 0 \\ 0 & m_2 & 0 \\ 0 & 0 & m_3 \end{pmatrix}, \qquad (13)$$

with $m_i \geq 0$. The unitary matrix U is defined as

$$U = \begin{pmatrix} U_{e1} & U_{e2} & U_{e3} \\ U_{\mu 1} & U_{\mu 2} & U_{\mu 3} \\ U_{\tau 1} & U_{\tau 2} & U_{\tau 3} \end{pmatrix} \begin{pmatrix} {\rm e}^{{\rm i}\phi_1} & 0 & 0 \\ 0 & {\rm e}^{{\rm i}\phi_2} & 0 \\ 0 & 0 & 1 \end{pmatrix}, \qquad (14)$$

where $\phi_{1,2}$ denotes the physical Majorana phases of the lepton sector. In the diagonal basis of charged lepton masses, U is just the MNS matrix. We can easily show that one Majorana phase connects cases (a1) and (a2), (b1) and (b2), and two Majorana phases connect the cases of (c1)–(c4). Thus, the stabilities of the mixing angles against quantum corrections are completely determined by three types of neutrino mass hierarchy (Type A, B, C) and two Majorana phases $\phi_{1,2}$ in stead of the classifications of (3)–(10).

We will analyze whether the lepton flavor mixing angles are changed or not by quantum corrections by fitting the low energy data. We determine the MNS matrix at the m_Z scale to be

$$U = \begin{pmatrix} \cos\theta_{12} & \sin\theta_{12} & 0 \\ -\frac{\sin\theta_{12}}{\sqrt{2}} & \frac{\cos\theta_{12}}{\sqrt{2}} & \frac{1}{\sqrt{2}} \\ \frac{\sin\theta_{12}}{\sqrt{2}} & -\frac{\cos\theta_{12}}{\sqrt{2}} & \frac{1}{\sqrt{2}} \end{pmatrix} \begin{pmatrix} {\rm e}^{{\rm i}\phi_1} & 0 & 0 \\ 0 & {\rm e}^{{\rm i}\phi_2} & 0 \\ 0 & 0 & 1 \end{pmatrix}, \qquad (15)$$

where we put $\sin\theta_{23} = 1/2^{1/2}$ and $\sin\theta_{13} = 0$, which values are suitable for the atmospheric neutrino experiments [2,3] and for the CHOOZ experiment [14], respectively. The mixing angle θ_{12} depends on the solar neutrino solutions of the large angle MSW solution (MSW-L), the small angle MSW solution (MSW-S) and the vacuum-oscillation solution (VO), which are given by[1]

$$\sin\theta_{12} = \begin{cases} 0.0042 \ (\theta = 0.0042) & \text{(MSW-S)}, \\ \frac{1}{\sqrt{2}} \quad \left(\theta = \frac{\pi}{4}\right) & \text{(MSW-L)}, \\ \frac{1}{\sqrt{2}} \quad \left(\theta = \frac{\pi}{4}\right) & \text{(VO)}. \end{cases} \qquad (16)$$

We also use the following values for the mass-squared differences in the numerical analyses:

$$\Delta m^2_{\rm solar} \simeq \begin{cases} 0.8 \times 10^{-5}\,{\rm eV}^2 & \text{(MSW-S)}, \\ 1.8 \times 10^{-5}\,{\rm eV}^2 & \text{(MSW-L)}, \\ 0.85 \times 10^{-10}\,{\rm eV}^2 & \text{(VO)}, \end{cases} \qquad (17)$$

$$\Delta m^2_{\rm ATM} \simeq 3.7 \times 10^{-3}\,{\rm eV}^2. \qquad (18)$$

The quantum corrections change the neutrino mass matrix; it is given by[2] [8,9]

$$\hat{\kappa}\,(m_R) = \frac{\hat{\kappa}\,(m_R)_{33}}{\kappa\,(m_Z)_{33}} \begin{pmatrix} 1-\epsilon & 0 & 0 \\ 0 & 1-\epsilon & 0 \\ 0 & 0 & 1 \end{pmatrix} \times \kappa\,(m_Z) \begin{pmatrix} 1-\epsilon & 0 & 0 \\ 0 & 1-\epsilon & 0 \\ 0 & 0 & 1 \end{pmatrix}, \qquad (19)$$

at the high energy scale m_R, where ϵ can be estimated to be

$$\epsilon \simeq 1 - \exp\left(-\frac{1}{16\pi^2}\int_{\ln(m_Z)}^{\ln(m_R)} y_\tau^2 {\rm d}t\right), \simeq \frac{1}{8\pi^2}\frac{m_\tau^2}{v^2}\left(1+\tan^2\beta\right)\ln\left(\frac{m_R}{m_Z}\right), \qquad (20)$$

[1] In the case of MSW-L, the mixing angle $\theta = \pi/4$ is not allowed by the experiments. However, a small deviation from the $\theta = \pi/4$ limit does not affect our analyses of the stability of the mixing angles with respect to quantum corrections

[2] Hereafter, we denote the mixing angles and the other physical parameters at the m_R scale by writing with the $\hat{}$ mark

Table 1. Stabilities of the mixing angles with the Type A mass hierarchy according to the change of ϕ_2 from 0 to π in the case of $m_R = 10^{13}$ GeV and $\tan\beta = 60$

	MSW-S	MSW-L	VO
$\sin^2 2\hat{\theta}_{12}$	0.005	0.998	0.998
$\sin^2 2\hat{\theta}_{23}$	0.985–0.99	0.985–0.99	0.99
$\sin^2 2\hat{\theta}_{13}$	10^{-7}	10^{-4}	10^{-10}

Table 2. Stabilities of the mixing angles with the Type B mass hierarchy according to a change of ϕ from 0 to π. In this analysis we use $m_R = 10^{13}$ GeV and $\tan\beta = 60$

	MSW-S	MSW-L	VO
$\sin^2 2\hat{\theta}_{12}$		See Figs. 1, 2	
$\sin^2 2\hat{\theta}_{23}$	0.99	0.99	0.99
$\sin^2 2\hat{\theta}_{13}$	0	0	0

where y_τ is the Yukawa coupling of τ, $v^2 \equiv v_u^2 + v_d^2$ and $\tan\beta \equiv v_u/v_d$ (v_u and v_d are the vacuum expectation values of the Higgs bosons, H_u and H_d, respectively). We neglect the Yukawa couplings of e and μ in (19) and (20), since those contributions to the renormalization group equations are negligibly small compared to that of τ [10]. The magnitude of ϵ can be determined by the value of $\tan\beta$ and the scale of m_R. The unitary matrix $\hat{U}$ which diagonalizes $\hat{\kappa}$ shows whether the lepton flavor mixing angles are stable against quantum corrections or not.

The value of ϵ is not large enough to change the neutrino mass matrix κ significantly [9,10]. Therefore, the neutrino mass matrix κ itself is stable against quantum corrections.

3 Type A ($m_1 \ll m_2 \ll m_3$)

In both the (a1) and the (a2) case, all mixing angles are stable against quantum corrections in each sign assignment [10]. This is understood from the analogy of the two-generation analysis, which shows that the mixing angle of the 2×2 mass matrix is not changed significantly by quantum corrections when there is a large mass hierarchy between the two neutrinos [10]. This situation is not changed when we consider the Majorana phase contribution as shown in the case of two-generation neutrinos [11]. The cases (a1) and (a2) are connected by the Majorana phase of ϕ_2, where ϕ_1 is rotated out, since $m_1 = 0$. The case of $\phi_2 = 0$ corresponds to (a1), while the case of $\phi_2 = \pi/2$ corresponds to (a2). Since Type A has a large mass hierarchy, all mixing angles are supposed to be stable against quantum corrections independently of the value of the Majorana phase ϕ_2. This is really confirmed by numerical analyses as shown in Table 1, where we use $m_R = 10^{13}$ GeV and $\tan\beta = 60$.

4 Type B ($m_1 \sim m_2 \gg m_3$)

In the Type B mass hierarchy, all mixing angles except for $\sin\theta_{12}$ of (b2) are stable against quantum corrections [10]. The analogy of the two-generation neutrino analysis shows that the mixing angles of $\sin\theta_{13}$ and $\sin\theta_{23}$ are stable against quantum corrections, since there are large mass hierarchies between the first and the third generation, and between the second and third generation. This is the same situation as that of Type A. This situation is not changed by including the Majorana phase contributions of $\phi_{1,2}$ as shown in Table 2, which shows the results of the numerical analyses in the case of $m_R = 10^{13}$ GeV and $\tan\beta = 60$. On the other hand, the mixing angle of θ_{12} can receive significant quantum corrections dependent on the relative sign assignment of m_2 as shown in [10]. The mixing angle of $\sin\theta_{12}$ of (b1) receives a quantum correction while that of (b2) does not. Now we understand that the two cases (b1) and (b2) are connected by the phase of $\phi \equiv \phi_1 - \phi_2$, which is the only physical phase, since $m_3 = 0$. The case of $\phi = 0$ corresponds to (b1), while the case of $\phi = \pi/2$ corresponds to (b2). The phase ϕ is the parameter which determines whether the mixing angle θ_{12} is stable against quantum corrections or not.

Now, let us show the analytic estimations of the stabilities of the mixing angles in the Type B mass hierarchy. The neutrino mass matrix of Type B which is diagonalized is given by

$$D_\kappa^{(\mathrm{B})} = m_1 \begin{pmatrix} 1 & 0 & 0 \\ 0 & 1+\xi_b & 0 \\ 0 & 0 & 0 \end{pmatrix}, \tag{21}$$

where

$$\xi_b \equiv \frac{m_2 - m_1}{m_1} \simeq \frac{1}{2}\frac{\Delta m^2_{\mathrm{solar}}}{\Delta m^2_{\mathrm{ATM}}}. \tag{22}$$

We can determine the mass matrix of $\kappa^{(\mathrm{B})}$ by using (12) and (15). Then (19) gives the mass matrix of $\hat{\kappa}^{(\mathrm{B})}$ at the high energy scale m_R.

The MNS matrix $\hat{U}^{(\mathrm{B})}$ which diagonalizes $\hat{\kappa}^{(\mathrm{B})}$ is given by

$$\hat{U}^{(\mathrm{B})} = \begin{pmatrix} 1 & 0 & 0 \\ 0 & (1-\epsilon)/\sqrt{1+(1-\epsilon)^2} & 1/\sqrt{1+(1-\epsilon)^2} \\ 0 & -1/\sqrt{1+(1-\epsilon)^2} & (1-\epsilon)/\sqrt{1+(1-\epsilon)^2} \end{pmatrix} \times \begin{pmatrix} \cos\hat{\theta}_{12} & \sin\hat{\theta}_{12} & 0 \\ -\sin\hat{\theta}_{12} & \cos\hat{\theta}_{12} & 0 \\ 0 & 0 & 1 \end{pmatrix} \begin{pmatrix} \mathrm{e}^{\mathrm{i}\hat{\phi}_1} & 0 & 0 \\ 0 & \mathrm{e}^{\mathrm{i}\hat{\phi}_2} & 0 \\ 0 & 0 & 1 \end{pmatrix}, \tag{23}$$

which means that the mixing angle between the first and the third generation, which is zero, is unchanged by quantum corrections. The mixing angle of $\hat{\theta}_{23}$ is given by

$$\sin^2 2\hat{\theta}_{23} = \left(\frac{2(1-\epsilon)}{1+(1-\epsilon)^2}\right)^2, \tag{24}$$

which indicates that the large mixing between the second and the third generation is stable with respect to

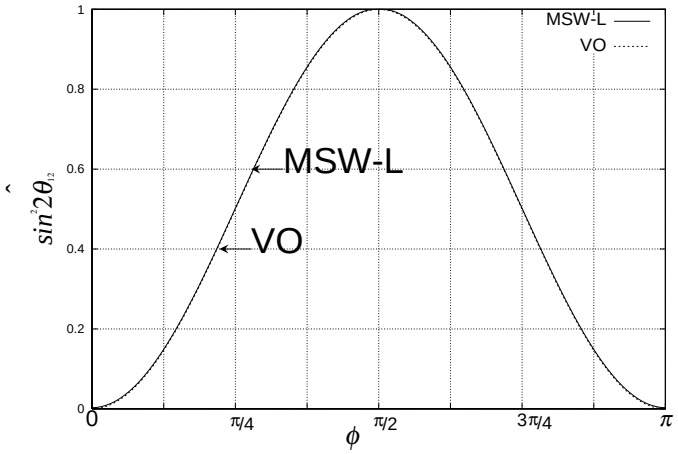

Fig. 1. Majorana phase dependence of $\sin^2 2\hat{\theta}_{12}$ for the MSW-L and the VO solutions in Type B mass hierarchy in the case of $m_R = 10^{13}$ GeV and $\tan\beta = 60$

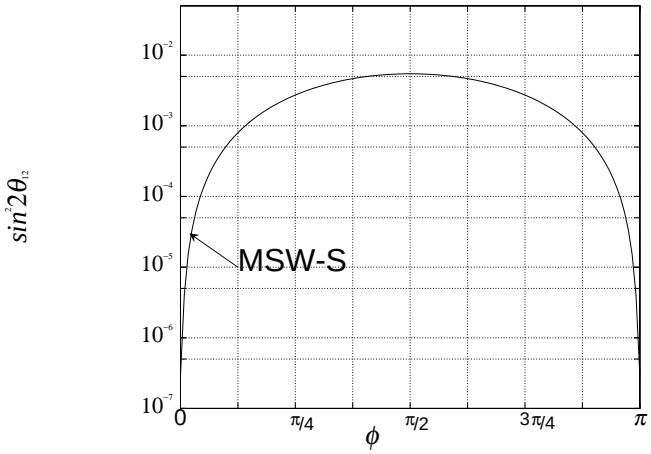

Fig. 2. Majorana phase dependence of $\sin^2 2\hat{\theta}_{12}$ for the MSW-S solution in the Type B mass hierarchy in the case of $\tan\beta = 60$ and $m_R = 10^{13}$ GeV

quantum corrections. By using (24), we can estimate that $\sin^2 2\hat{\theta}_{23} \simeq 0.99$ in the case of $m_R = 10^{13}$ GeV and $\tan\beta = 60$, which is consistent with the numerical analysis in Table 2. Therefore the mixing between the first and the third generation and the mixing between the second and the third generation are stable with respect to quantum corrections as shown in Table 2

How about the mixing between the first and the second generation?

For the MSW-L and the VO solutions, where $\sin\theta_{12} = \cos\theta_{12} = 1/2^{1/2}$ at the m_Z scale, the mixing angle of $\tan\hat{\theta}_{12}$ is given by

$$\tan 2\hat{\theta}_{12} \simeq (1-\epsilon)\sqrt{1-\epsilon}\frac{\sqrt{4\xi_b^2 + \epsilon^2 \sin^2 2\phi}}{\epsilon(1+\cos 2\phi)}, \quad (25)$$

where we use the approximation which neglects the higher order corrections of ϵ^2, $\epsilon\xi_b$, and ξ_b^2. When $\phi = \pi/2$, the mixing angle $\hat{\theta}_{12}$ becomes

$$\tan 2\hat{\theta}_{12} = \infty, \quad (26)$$

which means that the maximal mixing is stable against quantum corrections. On the other hand, when $\phi = 0$,

$$\tan 2\hat{\theta}_{12} \simeq \frac{\xi_b}{\epsilon}, \quad (27)$$

which shows that the mixing angle of $\hat{\theta}_{12}$ strongly depends on the magnitude of ϵ. The large mixing is spoiled when $\xi_b \leq \epsilon$, which corresponds to the region of $\tan\beta \geq 10$ for the MSW-L solution, and any value of $\tan\beta$ for the VO solution when we take $m_R = 10^{13}$ GeV. In Fig. 1, we show the change of $\sin^2 2\hat{\theta}_{12}$ due to the continuous change of the Majorana phase ϕ in the case of $\tan\beta = 60$ and $m_R = 10^{13}$ GeV. As the Majorana phase ϕ changes from 0 to $\pi/2$, the value of $\sin^2 2\hat{\theta}_{12}$ changes from 0 to 1. The large deviation from 1 of $\sin^2 2\hat{\theta}_{12}$ means that the mixing angle θ_{12} is unstable with respect to quantum corrections. Figure 1 shows that the mixing angle θ_{12} changes from being unstable to being stable as ϕ changes from 0 to π. The lines of the MSW-L and the VO solutions are almost overlapping in Fig. 1, since the discrepancy of the ξ_b's for the two solutions is negligible compared with the quantum correction, $\epsilon = 0.1$, when $\tan\beta = 60$ and $m_R = 10^{13}$ GeV.

As for the MSW-S solution, $\phi = 0$ induces

$$\tan 2\hat{\theta}_{12} \simeq \tan 2\theta_{12}\left(1 + \frac{1}{\cos 2\theta_{12}}\frac{\epsilon}{\xi_b}\right)^{-1}, \quad (28)$$

while $\phi = \pi/2$ induces

$$\tan 2\hat{\theta}_{12} \simeq \tan 2\theta_{12}. \quad (29)$$

Equations (28) and (29) show that the mixing angle of θ_{12} is not changed in the region of $\tan\beta \leq 10$ when $\phi = 0$, while it is not changed independently of $\tan\beta$ when $\phi = \pi/2$. The above conclusions are the same as those of [10]. In Fig. 2, we show the value of $\sin^2 2\hat{\theta}_{12}$ at the $m_R = 10^{13}$ GeV scale in the case of $\tan\beta = 60$ according to the continuous change of ϕ from 0 to π. Figure 2 shows that the mixing angle θ_{12} changes from being unstable to being stable corresponding to a change of ϕ from 0 to π.

5 Type C ($m_1 \sim m_2 \sim m_3$)

For the Type C mass hierarchy, it has been shown in [10] that the MNS matrix approaches a definite unitary matrix according to the relative sign assignments of the neutrino mass eigenvalues, as the effects of quantum corrections become large enough to neglect the mass-squared differences of the neutrinos. The independent parameters of the MNS matrix at the m_R scale approach the following fixed values in the large limit of quantum corrections:
case (c1): diag.$(-m_1, m_2, m_3)$

$$U_{e2} = \frac{\sin\theta_{12}}{\sqrt{1+\cos^2\theta_{12}}},$$

Table 3. The fixed values of the mixing angles for the MSW-L and the VO solutions in the large limit of quantum corrections given by (30)–(36)

	(c1)	(c2)	(c3)	(c4)
$\sin^2 2\hat{\theta}_{12}$	0.96	0.96	0.0	0.0
$\sin^2 2\hat{\theta}_{13}$	0.56	0.56	0.0	0.0
$\sin^2 2\hat{\theta}_{23}$	0.36	0.36	1.0	0.0

$$U_{e3} = -\frac{1}{2}\frac{\sin 2\theta_{12}}{\sqrt{1+\cos^2\theta_{12}}},$$
$$U_{\mu 3} = \frac{1}{\sqrt{2}}\frac{\sin^2\theta_{12}}{\sqrt{1+\cos^2\theta_{12}}}. \quad (30)$$

case (c2): diag.$(m_1, -m_2, m_3)$

$$U_{e2} = \sin\theta_{12},$$
$$U_{e3} = \frac{1}{2}\frac{\sin 2\theta_{12}}{\sqrt{1+\sin^2\theta_{12}}},$$
$$U_{\mu 3} = \frac{1}{\sqrt{2}}\frac{\cos^2\theta_{12}}{\sqrt{1+\sin^2\theta_{12}}}. \quad (31)$$

case (c3): diag.$(-m_1, -m_2, m_3)$

$$U_{e2} = 0, \quad U_{e3} = 0, \quad U_{\mu 3} = \frac{1}{\sqrt{2}}. \quad (32)$$

case (c4): diag.(m_1, m_2, m_3)

$$U_{e2} = 0, \quad U_{e3} = 0, \quad U_{\mu 3} = 0. \quad (33)$$

We can easily obtain the values of the mixing angles by using the relations of [15]:

$$\sin^2 2\theta_{12} = 4\frac{U_{e2}^2}{1-|U_{e3}|^2}\left(1-\frac{U_{e2}^2}{1-|U_{e3}|^2}\right), \quad (34)$$
$$\sin^2 2\theta_{13} = 4|U_{e3}|^2\left(1-|U_{e3}|^2\right), \quad (35)$$
$$\sin^2 2\theta_{23} = 4\frac{U_{\mu 3}^2}{1-|U_{e3}|^2}\left(1-\frac{U_{\mu 3}^2}{1-|U_{e3}|^2}\right). \quad (36)$$

As shown above, the cases of (c1)–(c4) are connected by the Majorana phases ϕ_1 and ϕ_2.

Figure 3 shows the values of the mixing angles at the high energy scale $m_R = 10^{13}\,\mathrm{GeV}$ for the MSW-L and the VO solutions according to continuous changes of the Majorana phases ϕ_1 and ϕ_2 in the case of $\tan\beta = 60$. Under the conditions that the effects of quantum corrections are large enough to neglect the mass-squared differences of the neutrinos, the results of the MSW-L solution are the same as those of the VO solution [10]. Table 3 shows the fixed values of the mixing angles for the MSW-L and the VO solutions in the large limit of quantum corrections which are obtained from (30)–(33) by using (34)–(36).

The deviations from the values at the m_Z scale, $\sin^2 2\theta_{12} = 1$, $\sin^2 2\theta_{13} = 0$ and $\sin^2 2\theta_{23} = 1$, indicate that the mixing angles receive significant quantum corrections. For $\sin^2 2\hat{\theta}_{12}$, Table 3 shows that the cases of (c1) and (c2) conserve maximal mixing, while the cases of (c3) and (c4) do not, in the large limit of quantum corrections. From (15), we can show that the change of ϕ_1 from 0 to $\pi/2$ with the relation $|\phi_2 - \phi_1| = 0$ ($|\phi_2 - \phi_1| = \pi/2$) corresponds to the change of (c4) to (c3) ((c2) to (c1)). Figure 3a shows that the unstable region of $\sin^2 2\hat{\theta}_{12} \lesssim 0.1$ occurs around the line of $|\phi_2 - \phi_1| = 0$, and the stable region of $\sin^2 2\hat{\theta}_{12} \sim 1.0$ is located around the line of $|\phi_2 - \phi_1| = \pi/2$. Since the cases of (c1) and (c2) have masses with opposite signs between the first and second generations, the mixing angle is stable from the analogy of two-generation neutrinos. Therefore, the maximal mixing between the first and second generation is conserved in the continuous region preserving the relation of $|\phi_2 - \phi_1| = \pi/2$. As for the stability of $\sin^2 2\hat{\theta}_{13}$, Table 3 shows that the cases of (c3) and (c4) conserve zero mixing, while the cases of (c1) and (c2) do not. Figure 3b shows that the stable region occurs around the line of $|\phi_2 - \phi_1| = 0$, which connects (c3) and (c4), and the unstable region is located around the line of $|\phi_2 - \phi_1| = \pi/2$, which connects (c1) and (c2). For the stability of $\sin^2 2\hat{\theta}_{23}$, Table 3 shows that the case of (c3) only conserves maximal mixing, and the case of (c4) induces zero mixing. The two cases of (c1) and (c2) induce $\sin^2 2\hat{\theta}_{23} \sim 0.36$. These situations are connected in a continuous manner by the two Majorana phases ϕ_1 and ϕ_2 as shown Fig. 3c.

Table 4. The fixed values of the mixing angles for the MSW-S solution in the large limit of quantum corrections given by (30)–(36)

	(c1)	(c2)	(c3)	(c4)
$\sin^2 2\hat{\theta}_{12}$	0.0	0.0	0.0	0.0
$\sin^2 2\hat{\theta}_{13}$	0.0	0.0	0.0	0.0
$\sin^2 2\hat{\theta}_{23}$	0.0	1.0	1.0	0.0

Figure 4 shows the values of the mixing angles at the high energy scale $m_R = 10^{13}\,\mathrm{GeV}$ for the continuous change of the Majorana phases for the MSW-S solution in the case of $\tan\beta = 60$. Table 4 shows the fixed values of the mixing angles for the MSW-S solution in the large limit of quantum corrections, which are obtained from (30)–(33) by using (34)–(36). The deviations from the values at the m_Z scale, $\sin^2 2\theta_{12} = 7.1 \times 10^{-5}$, $\sin^2 2\theta_{13} = 0$ and $\sin^2 2\theta_{23} = 1$, indicate that the mixing angles receive significant quantum corrections. For $\sin^2 2\hat{\theta}_{12}$, Table 4 shows that all the cases (c1)–(c4) make it zero in the large limit of quantum corrections. Figure 4a shows that the unstable region of $\sin^2 2\hat{\theta}_{12} > 0.2$ occurs around the points of $(\phi_1, \phi_2) \simeq (\pi/2, \pi/30)$ and $(\phi_1, \phi_2) \simeq (\pi/2, 29\pi/30)$. For the stability of $\sin^2 2\hat{\theta}_{13}$, Table 4 shows that all the cases (c1)–(c4) conserve zero mixing. Figure 4b shows that $\sin^2 2\hat{\theta}_{13}$ is stable with respect to quantum corrections for any values of the two Majorana phases. For the stability of $\sin^2 2\hat{\theta}_{23}$ Table 4 shows that the cases of (c2) and (c3) conserve maximal mixing, while the cases of (c1) and (c4) do not, in the large limit of quantum corrections. Figure 4c

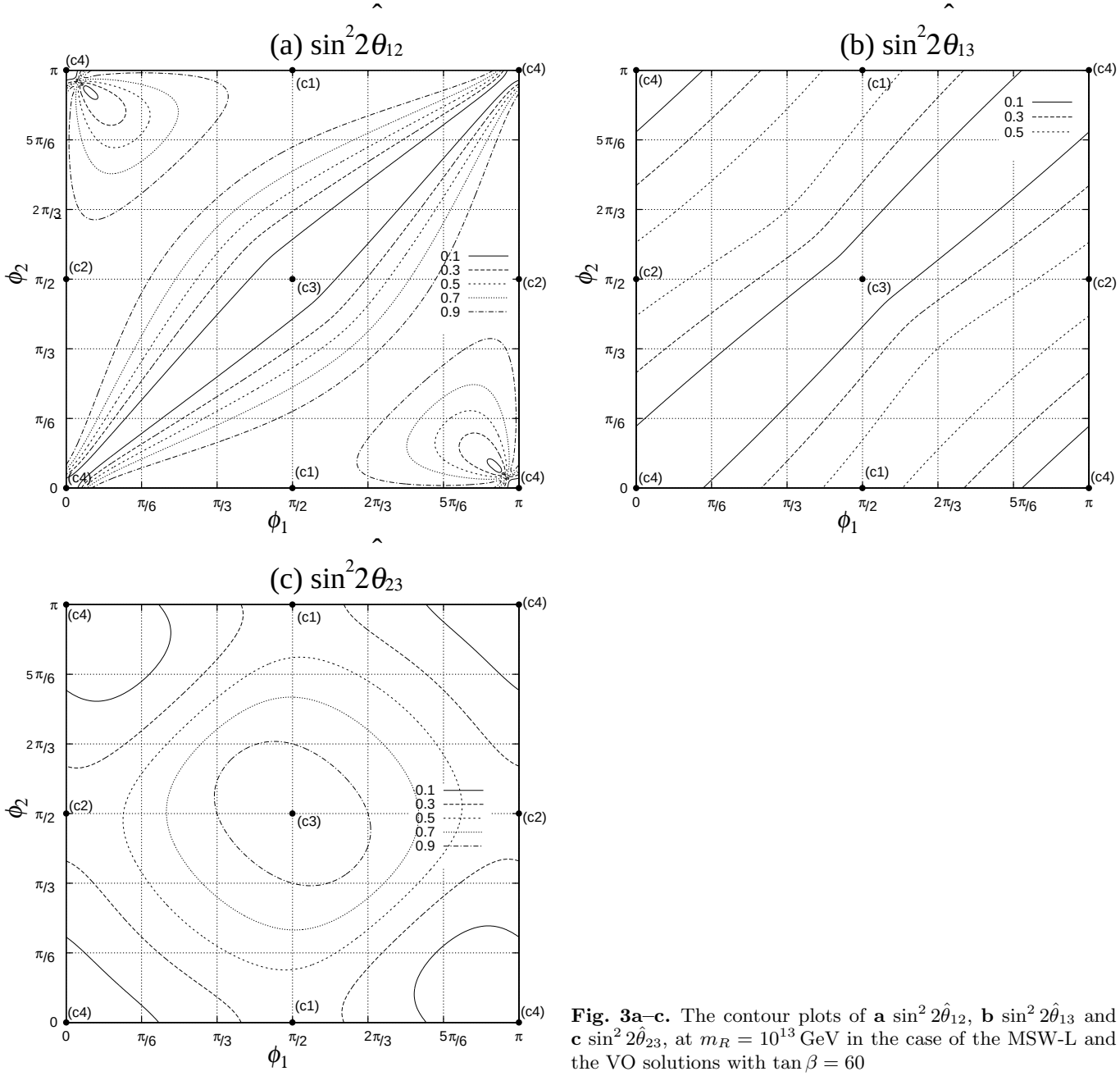

Fig. 3a–c. The contour plots of **a** $\sin^2 2\hat{\theta}_{12}$, **b** $\sin^2 2\hat{\theta}_{13}$ and **c** $\sin^2 2\hat{\theta}_{23}$, at $m_R = 10^{13}$ GeV in the case of the MSW-L and the VO solutions with $\tan\beta = 60$

shows that the stable region is located around the lines of $\phi_2 = \pi/2$, which connect (c2) and (c3) by changing ϕ_1 from 0 to $\pi/2$, and the unstable region occurs around the lines $\phi_2 = 0$ and $\phi_2 = \pi$, which connect (c1) and (c4) by changing ϕ_1 from 0 to $\pi/2$.

6 Summary

Neutrino-oscillation solutions for the atmospheric neutrino anomaly and the solar neutrino deficit can determine the texture of the neutrino mass matrix according to three types of neutrino mass hierarchy [13]: Type A: $m_1 \ll m_2 \ll m_3$, Type B: $m_1 \sim m_2 \gg m_3$, and Type C: $m_1 \sim m_2 \sim m_3$. We found that the relative sign assignments of the neutrino masses in each type of mass hierarchy play crucial roles in the stability against quantum corrections. Actually, two physical Majorana phases in the lepton flavor mixing matrix connect the relative sign assignments of the neutrino masses. Therefore, in this paper we analyze the stability of the mixing angles against quantum corrections according to three types of neutrino mass hierarchy (Type A, B, C) and two Majorana phases. The two phases play crucial roles in the stability of the mixing angles against quantum corrections. The results in [10], where the stabilities of the mixing angles in (a1) and (a2), (b1) and (b2), (c1)–(c4) with respect to quantum corrections are argued, are reproduced by taking definite values of the two Majorana phases.

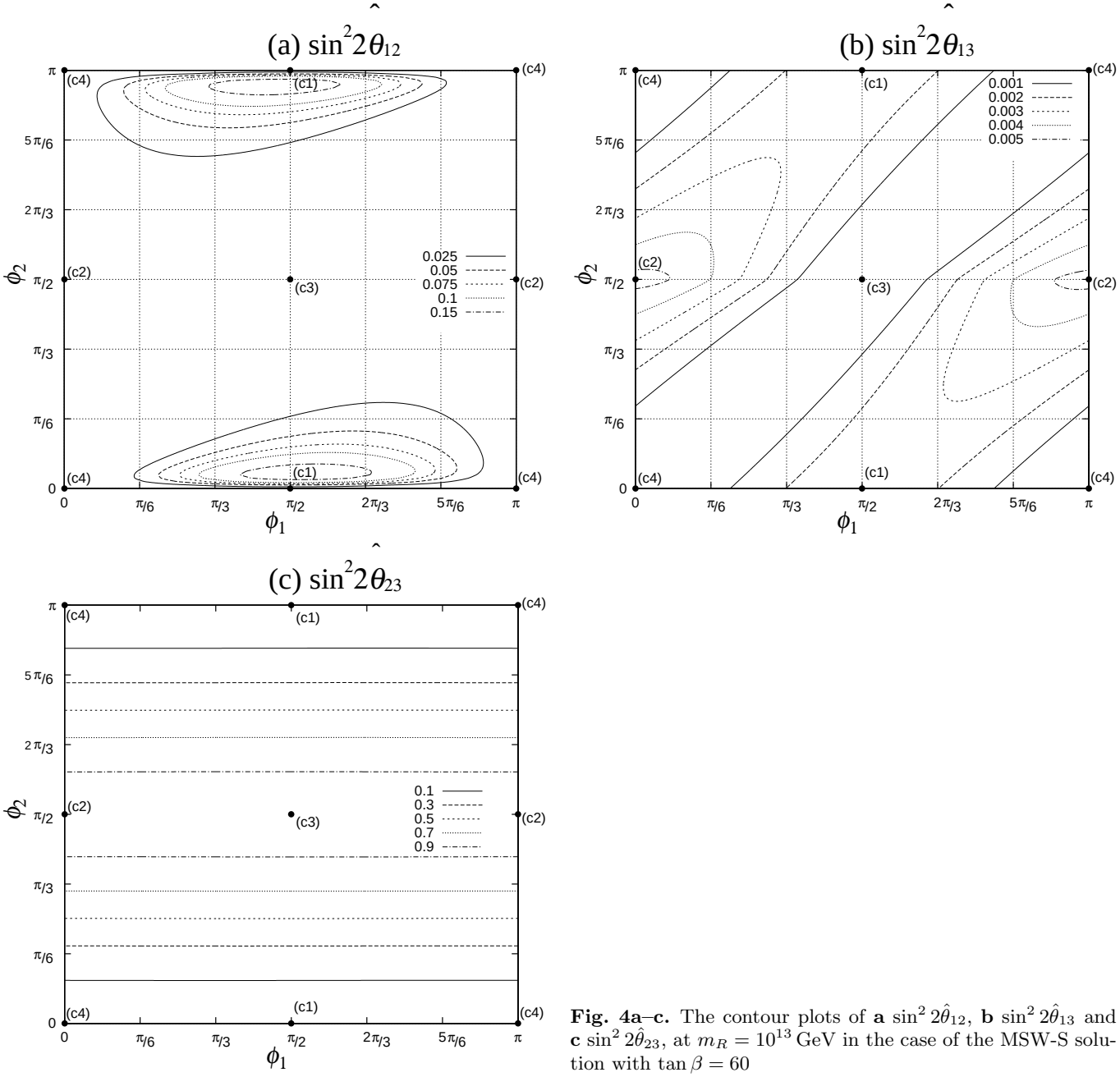

Fig. 4a–c. The contour plots of **a** $\sin^2 2\hat{\theta}_{12}$, **b** $\sin^2 2\hat{\theta}_{13}$ and **c** $\sin^2 2\hat{\theta}_{23}$, at $m_R = 10^{13}$ GeV in the case of the MSW-S solution with $\tan\beta = 60$

Acknowledgements. The work of NO is supported by the JSPS Research Fellowship for Young Scientists, No.2996.

References

1. Homestake Collaboration, B.T. Cleveland et al., Nucl. Phys. (Proc. Suppl.) B **38** (1995) 47; Kamiokande Collaboration, Y. Suzuki, Nucl. Phys. (Proc. Suppl.) B **38** (1995) 54; GALLEX Collaboration, P. Anselmann et al., Phys. Lett. B **357**, 237 (1995); SAGE Collaboration, J.N. Abdurashitov et al., Phys. Lett. B **328**, 234 (1994); Super-Kamiokande Collaboration, Phys. Rev. Lett. **82**, 1810 (1999); Phys. Rev. Lett. **82**, 2430 (1999); hep-ex/9903034
2. Kamiokande Collaboration, K.S. Hirata et al., Phys. Lett. B **205**, 416 (1988); ibid. B **280** (1992) 146; Y. Fukuda et al., Phys. Lett. B **335**, 237 (1994); IMB Collaboration, D. Casper et al., Phys. Rev. Lett. **66**, 2561 (1991); R. Becker-Szendy et al., Phys. Rev. D **46**, 3720 (1992); SOUDAN2 Collaboration, T. Kafka, Nucl. Phys. (Proc. Suppl.) B **35** (1994) 427; M.C. Goodman, ibid. **38** (1995) 337; W.W.M. Allison et al., Phys. Lett. B **391**, 491 (1997); Phys. Lett. B **449**, 137 (1999)
3. Y. Totsuka, invited talk at the 18th International Symposium on Lepton–Photon Interaction, July 28–August 1, 1997 Hamburg; Super-Kamiokande Collaboration, Phys. Rev. Lett. **81**, 1562 (1998); Phys. Rev. Lett. **82**, 2644 (1999); hep-ex/9903047; hep-ex/9905016; Phys. Lett. B **467**, 185 (1999)
4. Z. Maki, M. Nakagawa, S. Sakata, Prog. Theor. Phys. **28**, 870 (1962)

5. P.H. Chankowski, Z. Pluciennik, Phys. Lett. B **316**, 312 (1993); K.S. Babu, C.N. Leung, J. Pantaleone, Phys. Lett. B **319**, 191 (1993)
6. M. Tanimoto, Phys. Lett. B **360**, 41 (1995); J. Ellis, G.K. Leontaris, S. Lola, D.V. Nanopoulos, Eur. Phys. J. C **9**, 389 (1999); S. Lola, hep-ph/9903203; J.A. Casas, J.R. Espinosa, A. Ibarra, I. Navarro, Nucl. Phys. B **556**, 3 (1999), Nucl. Phys. B **569**, 82 (2000); JHEP **9**, 015 (1999); Yue-Liang Wu, hep-ph/9905222; M. Carena, J. Ellis, S. Lola, C.E.M. Wagner, Eur. Phys. J. C **12**, 507 (2000); R. Barbieri, G. Ross, A. Strumia, JHEP **10**, 20 (1999); E. Ma, J.Phys. G **25**, L97 (1999), hep-ph/9907503; K.R.S. Balaji, A.S. Dighe, R.N. Mohapatra, M.K. Parida, hep-ph/0001310, hep-ph/0002177
7. N. Haba, N. Okamura, M. Sugiura, Prog. Theor. Phys. **103**, 367 (2000)
8. J. Ellis, S. Lola, Phys. Lett. B **458**, 310 (1999)
9. N. Haba, Y. Matsui, N. Okamura, M. Sugiura, Eur. Phys. J. C **10**, 677 (1999)
10. N. Haba, N. Okamura, hep-ph/9906481 to be published in Eur. Phys. J. C
11. N. Haba, Y. Matsui, N. Okamura, M. Sugiura, Prog. Theor. Phys. **103**, 145 (2000)
12. N. Haba, Y. Matsui, N. Okamura, Prog. Theor. Phys. **103**, 807 (2000)
13. G. Altarelli, F. Feruglio, JHEP **11**, 21 (1998)
14. M. Apollonio et al., The CHOOZ Collaboration, Phys. Lett. B **466**, 415 (1999); hep-ex/9910042
15. K. Hagiwara, N. Okamura, Nucl. Phys. B **548**, 60 (1999)